Absorption and Transport Effects Induced in Plasmas by the Interaction of Electrons with Laser Speckles

M. Sherlock and P. Michel
Lawrence Livermore National Laboratory, California 94551, United States

(Received 17 March 2022; revised 21 September 2022; accepted 3 October 2022; published 16 November 2022)

We show that the ponderomotive force associated with laser speckles can scatter electrons in a laser-produced plasma in a manner similar to Coulomb scattering. Analytic expressions for the effective collision rates are given. The electron-speckle collisions become important at high laser intensity or during filamentation, affecting both long- and short-pulse laser intensity regimes. As an example, we find that the effective collision rate in the laser-overlap region of hohlraums on the National Ignition Facility is expected to exceed the Coulomb collision rate by 1 order of magnitude, leading to a fundamental change to the electron transport properties. At the high intensities characteristic of short-pulse laser-plasma interactions ($I \gtrsim 10^{17}$ W cm^{-2}), the scattering is strong enough to cause the direct absorption of laser energy, generating hot electrons with energy scaling as $E \approx 1.44(I/10^{18}\ \mathrm{W\,cm^{-2}})^{1/2}$ MeV, close to experimentally observed results.

DOI: 10.1103/PhysRevLett.129.215001

Intense lasers are used in the laboratory to generate plasmas as a route to understanding the physics of high energy-density systems, with applications ranging from inertial confinement fusion (ICF) and particle acceleration to laboratory studies of astrophysics. The dominant electron transport processes that describe the flow of thermal energy and magnetic field in the plasma are mediated by Coulomb collisions between electrons and ions [1]. In this Letter, we show that electrons can also undergo scattering with the laser electromagnetic field, which introduces an additional collisionality to the plasma and modifies the transport properties. Modern high-power lasers use smoothing techniques, such as random phase plates [2] and smoothing by spectral dispersion (SSD) [3], to produce smooth intensity profiles at large spatial and temporal scales (relative to hydrodynamic scales), thereby limiting the growth of hydrodynamic instabilities. However, laser intensity profiles still exhibit small-scale time-dependent intensity nonuniformities (*speckles*) whose size and lifetime are determined by the smoothing technique, typically characterized by spatial scales of a few microns and timescales of a few picoseconds. Each speckle exerts a ponderomotive force on the electrons which acts to scatter them. The electrostatic field induced in the plasma by the speckles acts in a similar way and may cause additional scattering, depending on the circumstances. The cumulative effect of electrons interacting with multiple speckles results in the loss of electron directed momentum. In some important applications, such as the laser-overlap region in ICF hohlraum plasmas, electron-speckle collisions can dominate over Coulomb collisions. Fig. 1 shows a conceptual illustration of this process for a simple two-beam hohlraum, with an example stochastic electron trajectory represented by the cyan curve (labeled "e"). In this Letter, we derive the rate of directed momentum loss and show how it affects electron transport and laser absorption. Applying the theory to the region of crossing beams on the National Ignition Facility (NIF) laser, we estimate a reduction in the electron thermal conductivity by a factor of ≈ 20. Understanding the plasma conditions in the laser overlap region in hohlraums is important because this region determines the energy transfer between beams by the cross beam energy transfer effect [4–6] and the growth rates for laser filamentation [7,8], which in turn determine the symmetry of the radiation drive onto the capsule. The plasma conditions are primarily determined by the inverse bremsstrahlung absorption (a process that is relatively well understood, see e.g., Ref. [9]) and thermal transport in the kinetic regime [10,11]. Given the dominance of electron-speckle collisions, we make the case that these interactions should also be considered for a complete description of heat flow.

If the electromagnetic wave is speckled, the Lawson-Woodward theorem [12] no longer applies, and when the intensity approaches relativistic ($I \gtrsim 4 \times 10^{17}$ W cm^{-2}) electrons can gain energy from the laser directly, without the involvement of space-charge fields. This effect can be motivated phenomenologically by making an analogy with inverse-bremsstrahlung absorption [9], in which the average thermal momentum of electrons, $\langle \Delta p^2 \rangle$ is related to the oscillatory momentum p_{osc} via $d\langle \Delta p^2 \rangle / dt \approx \upsilon_p p_{\mathrm{osc}}^2$, where υ_p is the effective collision rate for electrons interacting with speckles. As with inverse bremsstrahlung, electrons gain energy because of the change in phase

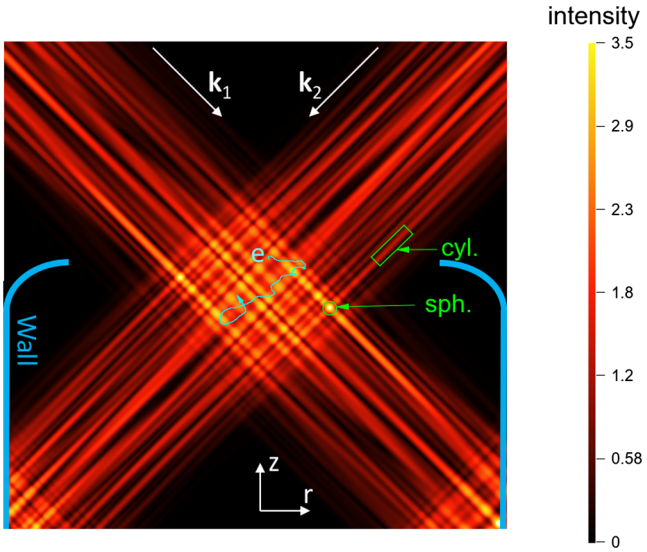

FIG. 1. A simple hohlraum illuminated by two speckled laser beams (with incident k vectors $\mathbf{k}_1$ and $\mathbf{k}_2$). Speckles approximated with cylindrical ("cyl.") and spherical ("sph.") symmetry are shown. The colorbar corresponds to the laser intensity (normalized to the average), and the cyan curve (labeled "e") shows an example electron trajectory.

induced by the collision. As a result of the effective collisionality introduced by speckles, the accelerated electron spectrum is expected to be quasithermal, as observed in experiments [13–17].

To derive the electron-speckle collision rates, we use an analogy with electron-ion Coulomb scattering, replacing the ions with speckles. A laser speckle with intensity I encountered by an electron moving in the x-y plane is approximated by an intensity profile with ponderomotive potential of the form $\varphi_p = \frac{1}{4} m v_{\rm osc}^2 \{1 - [(x^2 + y^2)/R^2]\}$, where $v_{\rm osc} = eE_0/m\omega_0$ is the electron oscillatory velocity in the laser field of frequency ω_0, $E_0 = \sqrt{2I/c\epsilon_0}$ is the peak laser electric field strength, and R is the speckle radius. One can consider a correction factor of order unity to this potential to account for the electrostatic response of the plasma to the SSD, and kinetic effects (discussed below). The equation of motion of an electron in this potential is $m d^2\mathbf{r}/dt^2 = -\nabla\varphi_p$. In reference to Fig. 6, an electron incident on the speckle with impact parameter $b = y(0)$ at $x(0) = x_0 = -\sqrt{R^2 - b^2}$ and initial velocity v in the x direction has solutions $x(t) = \frac{1}{2} e^{\omega t}(v/\omega - x_0) - \frac{1}{2} e^{-\omega t}(\mathrm{v}/\omega + x_0)$ and $y(t) = \frac{1}{2} b(e^{\omega t} + e^{-\omega t})$, where $\omega = v_{\rm osc}/\sqrt{2}R$. The electron is scattered by the speckle through angle θ, returning to the initial radius R at time $t_R = \ln(W_+/W_-)/(R/\sqrt{2}v_{\rm osc})$, where $W_\pm = R v_{\rm osc}^2 \pm 2\sqrt{2(R^2 - b^2)}\, v_{\rm osc}\mathrm{v} + 2R\mathrm{v}^2$. The angle θ can be found from the electron velocity at $t = t_R$: $\theta = \arctan\{2bx_0 v_{\rm osc}^2/[2b^2 v_{\rm osc}^2 + (2\mathrm{v}^2 - v_{\rm osc}^2)R^2]\}$. Since the scattering angle is known, we can calculate the directed momentum-loss rate [18] ν_p defined via the equation $\langle \Delta v_x/\Delta t\rangle_b = -\nu_p v_x$, where Δv_x is the change in the electron velocity along its initial direction (v_x) in time Δt. The angular parentheses $\langle\ldots\rangle_b$ denote an average over all impact parameters. The directed momentum loss of an electron with impact parameter b, after the interaction with a single speckle of intensity $I \propto v_{\rm osc}^2$ and radius R, is $m\Delta v_x = m v_x(1 - \cos\theta)$. The integration over the impact parameter depends on the speckle shape, and we consider two limits: when the beam is tightly focused (corresponding to beam F number $F = 1$) or multiple beams overlap, we treat the speckles as spherically symmetric, with rates denoted by subscript "s" ($\nu_{p,s}$ etc), and when the beam is straight ($F = \infty$), speckles are treated as potentials with cylindrical symmetry, with rates denoted by subscript "c". Examples of cylindrical and spherical speckles are indicated in Fig. 1. In the case of cylindrical speckles, only the electrons moving perpendicular to the beam direction are heavily scattered, but in the case of spherical speckles the scattering is isotropic. The case of spherical scatterers is deferred to the Supplemental Material [19]; here we focus on the cylindrical case. In time Δt, cylindrical scatterers with number n_A per unit area will undergo velocity change $\Delta v_x = \int_0^R v_x(1 - \cos\theta) n_A \mathrm{v}\Delta t db$. Carrying out the integral gives $\nu_{p,c}(w, v_{\rm osc}) = 24w^3 - 4w - \sqrt{2}(12w^4 - 4w^2 - 1)\ln\Lambda(w) n_A R v_{\rm osc}/(32w^2)$, where $\Lambda = (2w^2 + 2\sqrt{2}w + 1)/(2w^2 - 2\sqrt{2}w + 1)$, and $w = v_x/v_{\rm osc}$. This expression for $\nu_{p,c}$ can be simplified by carrying out a fit to a rational approximant. We choose a fitting function of the form $g(w) = p_1 w/(1 + p_2 w^4)$, which is the simplest function exhibiting the same dependence on w in the small ($w \ll 1$) and large ($w \gg 1$) limits. The coefficients p_i are found by equating the coefficients of the first-order Taylor (in w) and asymptotic (in $1/w$) expansions of $\nu_{p,c}(w, v_{\rm osc})$ with the coefficients of the same expansions of $g(w)$, giving $\tilde{\nu}_{p,c}(w, v_{\rm osc}) \simeq \frac{4}{3} n_A R v_{\rm osc} w/(1 + 20w^4)$ as an approximate form for $\nu_{p,c}$. This agrees well with the full expression for $\nu_{p,c}$ in the range $0.15 \gtrsim w \gtrsim 1$.

In the Appendix we average $\tilde{\nu}_{p,c}$ over the speckle intensity distribution giving

$$\tilde{\nu}_{p,c}(v) = \frac{4}{3\pi R} \frac{v}{1 + a_c (v/v_0)^4} \tag{1}$$

where $a_c \approx 1.1$. In order for multiple scattering to apply, we require the mean-free path of electrons $\lambda_{\rm mfp} = v/\tilde{\nu}_{p,c/s}(v)$ to exceed the speckle size. In most regimes of interest for transport, $v \gg v_0$, and in this limit $\lambda_{\rm mfp} = (3\pi R/4) a_{c/s} (v/v_0)^4 \gg R$. Eq. (1) can be further averaged over a Maxwellian velocity distribution (see the Appendix) and expressed in practical units:

$$\nu_{p,c,M} \approx I_{15}^2 \lambda_3^4 R_{\mu m}^{-1} T_{keV}^{-3/2} \ln(46 T_{keV} I_{15}^{-1} \lambda_3^{-2}) 4.3 \times 10^9 \ s^{-1} \quad (2)$$

where I_{15} is the average laser intensity in units of 10^{15} W cm^{-2}, λ_3 the laser wavelength in units of 0.351 μm, T_{keV} the electron temperature in units of keV, and $R_{\mu m}$ the speckle radius in μm.

At intensities of $\sim 10^{15}$ W cm^{-2}, the effective collision rates are relatively weak, but some important applications in ICF involve high intensities. For example, taking conditions representative of the laser entrance hole region in hohlraums on the NIF laser ($n_e \approx 0.05 n_c$, $T_e \approx 5$ keV, $Z \approx 2$) [10], where 96 overlapping beams [26] generate speckles at the wavelength scale $\lambda_0 = 0.351$ μm, with average intensity $\approx 2.4 \times 10^{16}$ W cm^{-2}, we find $\nu_{p,s,M} \approx 1 \times 10^{12}$ s^{-1}. This estimate is over 1 order of magnitude greater than the Coulomb collision rate ($\approx 4.5 \times 10^{10}$ s^{-1}), indicating electron-speckle collisions may be the dominant scattering mechanism. The collision rate relative to the Coulomb rate ($\nu_{p,c,M}/\upsilon_{ei}$) is plotted as a function of intensity in Fig. 2 for the NIF conditions and a typical scenario relevant to the OMEGA laser ($n_e \approx 0.1 n_c$, $T_e \approx 3$ keV, $Z \approx 5.3$, $R \approx 3$ μm).

When the ponderomotive force acts on the plasma, an electrostatic field is also generated, and we consider now the characteristics of this field. In the case of a time-independent intensity, the electrostatic field can be determined by the force balance between the ponderomotive force $\boldsymbol{F}_p = -e^2/(4m\omega_0^2)\nabla|\boldsymbol{E}_0(\boldsymbol{r})|^2$ and the plasma pressure gradient $-T_e \nabla n_e/n_e$, where n_e is the electron number density, T_e is the electron temperature (assumed uniform), e is the electron charge, m is the electron mass, ω_0 is the laser frequency, $\mathbf{E}_0$ the electric field of the laser, and I the intensity. The velocity-averaged electron equation of motion is $m_e d\mathbf{u}_e/dt = -e\boldsymbol{E} - T_e \nabla n_e/n_e + \boldsymbol{F}_p$, where $\mathbf{E}$ is the electrostatic field and $\mathbf{u}_e$ is the average electron velocity. The effect of the laser field has been averaged over the laser cycle and is included only in the term $\boldsymbol{F}_p$, while the field $\mathbf{E}$ results from charge separation. The ions reach equilibrium by balancing the induced electric field with the ion pressure gradient: $m_i d\boldsymbol{u}_i/dt = Ze\boldsymbol{E} - T_i \nabla n_i/n_i$, where Z is the ion charge. In equilibrium these equations can be combined, assuming quasineutrality $n_e \simeq Z n_i$, to show $\mathbf{E} = (1 + ZT_e/T_i)^{-1} \boldsymbol{F}_p/e$, i.e., the speckle induces a field with spatial characteristics closely related to its intensity profile. However, this analysis ignores time dependence associated with the SSD. In the Supplemental Material [19] we describe Vlasov-Fokker-Planck simulations that account for this effect, resulting in a similar scaling for the induced field: $\mathbf{E} \approx \alpha \boldsymbol{F}_p/e$, where α is a parameter, determined by the simulations, lying in the range $0.5 \lesssim \alpha \lesssim 2$. The field $\mathbf{E}$ therefore adds corrections of order α to the theory.

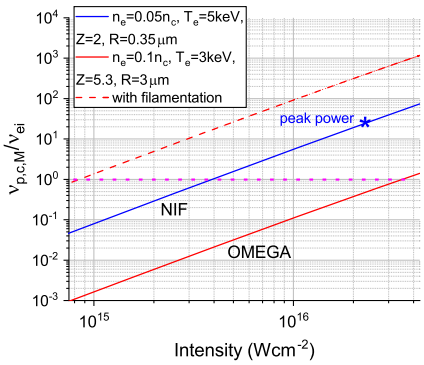

FIG. 2. The speckle collision rate relative to the Coulomb rate ($\nu_{p,c,M}/\upsilon_{ei}$) as a function of laser intensity. The intensity in the laser overlap region on the NIF is indicated by the asterisk (*). The dashed red line corresponds to the same conditions as the red line but accounts for thermal filamentation.

The effect on electron transport can be estimated from the $v \gg v_0$ limit of Eq. (1), $\tilde{\nu}_{p,s}(v) \approx 4v_0^4/(a_s 3\pi R v^3)$, which represents the directed momentum loss rate of the electons involved in determining most transport coefficients of interest ($v_t \lesssim v \lesssim 5v_t$), including the important effects of thermal conductivity and Nernst convection [1]. Low velocity effects such as electron-ion thermal equilibration and collisional damping of ion acoustic waves are unaffected due to the dominance of Coulomb scattering. Since this form for $\tilde{\nu}_{p,s}$ has the same dependence on velocity as electron-ion Coulomb scattering (v^{-3}), the effect of electron scattering with spherical speckles can be approximately accounted for by making the replacement $\nu_{ei} \to \nu_{ei} + \nu_{p,s,M}$ in the coefficients, where ν_{ei} is the Maxwellian-averaged electron-ion Coulomb collision rate and $\nu_{p,s,M}$ is given in the Supplemental Material [19]. For example, the thermal conductivity $\kappa \propto 1/\nu_{ei}$ is straightforwardly replaced with $\kappa \propto 1/(\nu_{ei} + \nu_{p,s,M})$. Note that for cylindrical speckles, the thermal conductivity is only affected in the direction perpendicular to the laser k vector ($\mathbf{k}$), so only the perpendicular conductivity $\kappa_\perp$ is modified: $\mathbf{q} = \kappa_\perp \mathbf{k} \times (\nabla T_e \times \mathbf{k})$. According to the above discussion, we would therefore expect a reduction in the effective thermal conductivity in the NIF laser entrance hole region by a factor of ≈ 20.

We have so far neglected processes that can significantly alter the characteristics of the speckles and induced fields, notably the refraction of speckled light at oblique incidence [27] and thermal filamentation [7,28]. The latter effect can enhance the scattering rate substantially. The ponderomotively induced electrostatic field ($\mathbf{E} \approx \mathbf{F}_p/e$) associated with an average laser intensity of 10^{15} W cm^{-2} and speckles of radius $R_0 = 3$ μm has root mean square (rms) magnitude $\approx 10^7$ Vm^{-1}, which is the field strength expected in the absence of filamentation. The field associated with density perturbations driven by filamentation is $|\mathbf{E}| = -\nabla P_e/en_e \approx (\delta n_e/n_e) T_e/Re$, where R is the speckle radius

after filamentation. Considering the typical density perturbation associated with a speckle ($\delta n_e/n_e \approx 0.1$) is approximately doubled during filamentation ($\delta n_e/n_e \approx 0.2$) so that $R \approx R_0/2$, and assuming the number of filaments approximately doubles as the beam breaks up results in an increase in the rms field strength by a factor of ≈ 25. The electron-speckle collision rate ($\propto E^2/R$) therefore increases by a factor of $\approx 10^3$, which makes it comparable to the Coulomb collision rate for a CH plasma at $I = 10^{15}$ W cm^{-2}. The dashed red line in Fig. 2 corresponds to the OMEGA laser conditions but with the inclusion of this estimate for the enhancement caused by filamentation.

Speckles are also a common feature of laser-matter interactions at relativistic intensities [29,30], and in many ways they are unavoidable due to the difficulty of maintaining perfectly smooth targets and beams throughout the pulse. They invalidate the plane wave approximation, but their effect has until now been unexplored theoretically in this regime. Using the relativistic formula derived in the Appendix for the case of $\lambda_0 = 1$ μm, $I = 10^{18}$ W cm^{-2} and an electron with momentum $p = mc$, we find a collision time of just $\nu^{-1}_{p,s,\mathrm{rel}} \approx 8$ fs, which is comparable to the laser period. The large magnitude of this collisionality indicates the perturbations induced by speckles on the electron trajectory are non-negligible. Particle-in-cell simulations of electron acceleration in the underdense plasma frequently show energetic ($E \lesssim 1$ MeV) electrons undergoing stochastic motion in the corona (see, e.g., Ref. [15]), and this behavior is consistent with our 8 fs estimate for the collision time. The collisions have the undesirable effect of increasing the electron beam divergence angle, which is a key metric for most applications (e.g., x-ray backlighting) and a crucial parameter in the fast ignition approach to inertial fusion [31]. The decreased scattering rate of the higher energy electrons predicted by our theory may explain why higher energy electrons are emitted with a reduced divergence angle [32].

To study electron energy gain at relativistic intensities, we consider a Gaussian plane wave reflecting off a nonuniform critical surface, which generates a speckled reflected wave. The electric field (E_x) in this scenario is plotted in Fig. 3. The wavelength is $\lambda_0 = 1$ μm, the peak incident intensity is 4×10^{17} W cm^{-2}, and the critical surface is assumed to generate a speckled beam (moving in the $-z$ direction) with Gaussian statistics whose mean radius is 1 μm. For illustrative purposes, the Gaussian envelope on each beam in Fig. 3 has a relatively short full-width half-max length of 10 μm, and the envelopes on the incident and reflected waves are centered on $z = -5$ μm and $z = 5$ μm, respectively. The oscillatory energy of electrons in the incident plane wave can be thermalized by the interaction with the reflected, speckled beam, resulting in a nonadiabatic interaction of the electrons with the beams. The speckles can be thought of as introducing a stochastic force, and the presence of even small stochastic

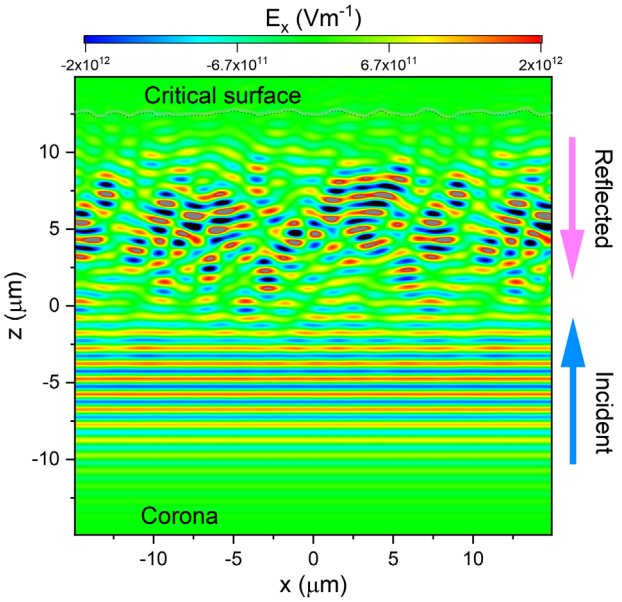

FIG. 3. The electric field (E_x) that results from the interference of an incident Gaussian plane wave (moving in the z direction) reflecting off a nonuniform critical surface.

forces is well known to lead to energy transfer at high intensity [33]. Although the case of two plane waves interacting does lead to absorption due to the nonlinearity of the interaction [34] at intensities $\gtrsim 10^{18}$ W cm^{-2}, accounting for speckles leads to much greater energy gains even at relatively low intensity ($\gtrsim 10^{17}$ W cm^{-2}). We have studied this process numerically by integrating the electron equations of motion in the laser interference fields. We do not include the electrostatic field generated by the plasma in order to clearly demonstrate large energy gain can be produced by the laser fields alone. An example of the energy gained is shown in Fig. 4(a) for the case of two Gaussian pulses each with FWHM pulse length of 300 fs and intensity $I = 4 \times 10^{17}$ W cm^{-2}, initially separated by a large distance, interacting with electrons initially located at the midpoint of the two beams with temperature 16 keV. For comparison, the case of two uniform beams is also shown. The average energy gained by the electrons is ≈ 0.22 MeV for the case with speckles, significantly above the ponderomotive scaling [29] ($T_{\mathrm{pond}} \approx 0.07$ MeV) and a factor of ≈ 6 greater than the case with uniform beams. Quasithermal electron energy spectra are generated, shown in Fig. 4(b) with a comparison to T_{pond}. In Fig. 5 we show the hot electron energy scaling from these simulations for a range of intensities, along with recent experimental measurements at relatively low intensity [15,16].

In order for electrons to gain energy from a pump wave via electron-speckle scattering, the deflection has to occur on timescales comparable to or shorter than the oscillation period in the pump [9]. This becomes the case at relativistic intensities for small scale speckles ($R \approx \lambda_0$). The thermal

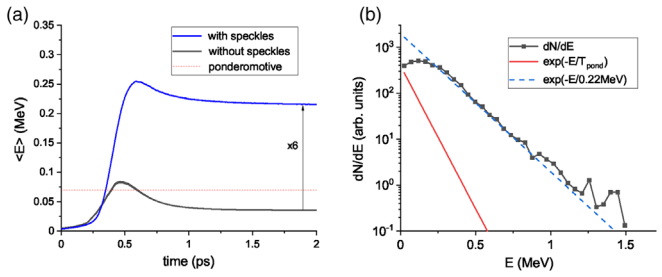

FIG. 4. (a) Average electron energy as a function of time and (b) final electron energy spectrum for two interfering 300 fs pulses with peak intensity 4×10^{17} W cm^{-2} and $\lambda_0 = 1$ μm.

energy gain scaling can be estimated by considering the simplified scenario in which an electron is moving in the direction of the pump, so that the pump oscillation time is long compared with the speckle interaction time and the collision can be assumed to be instantaneous. We decompose the electron momentum $\mathbf{w}$ into components $\mathbf{w} = \mathbf{p} + \mathbf{u}$, where $\mathbf{p}$ is the thermal momentum and $\mathbf{u}$ is the oscillatory momentum in the pump, and consider the square change in thermal momentum $\Delta(p^2)$ in time Δt when scattering through angle θ: $\Delta(p^2)/\Delta t = 2\boldsymbol{u}.\boldsymbol{w}(1-\cos\theta) - uw\sin\theta\cos\phi\sin\theta'$, where θ' is the angle between $\boldsymbol{u}$ and $\boldsymbol{w}$ and ϕ is the azimuthal angle. The term in ϕ can be neglected due to symmetry. The scattering angle is expressed in terms of the impact parameter $\theta(b)$ and as above we integrate over all impact parameters, assuming $v \approx c$, $\Delta(p^2)/\Delta t = 2\boldsymbol{u}.\boldsymbol{w}\int_0^R [1-\cos\theta(b)] n_s 2\pi v b db = 2(u^2 + 2up\cos\chi) n_s I_1 v$, where $n_s = (4\pi R^3/3)^{-1}$ is the density of speckles, χ is the angle between $\mathbf{u}$ and $\mathbf{p}$, and $I_1 = \int_0^R [1-\cos\theta(b)] 2\pi b db$ follows a similar form to the nonrelativistic case $I_1 \approx \pi R^2/(1+12\bar{v}^4)$, with $\bar{v}^2 \approx w/u_{\mathrm{osc}}$ and $u_{\mathrm{osc}} = e\sqrt{2I/c\varepsilon_0}/\omega_0$ the peak oscillatory momentum in the speckle at intensity I (assumed equal to the pump intensity). Averaging over all solid angles gives $\Delta(p^2)/\Delta t = 2u^2 n_s I_1 c$. For electrons with initially low energy $w/u_{\mathrm{osc}} \ll 1$, the cross section is $I_1 \approx \pi R^2$, i.e., the speckles are effective scatterers. In the time $\boldsymbol{\Delta t}$, assumed short in comparison to the relatively long oscillatory time in a relativistic pump, the oscillatory momentum gained from the pump averaged over all laser phases is $u \approx eE_0\boldsymbol{\Delta} t/2$ (see Appendix), where $E_0 = \sqrt{2I/c\varepsilon_0}$ is the peak electric field of the pump. Considering a deflection timescale equal to the speckle crossing time R/c, and a speckle size $R = \lambda_0$, the thermal energy gain is $E \approx \sqrt{\Delta(p^2)}c = \sqrt{3/2}\pi a_0 mc^2$ per interaction, where $a_0 = eE_0/mc\omega_0$ is the normalized vector potential of the pump. Once the energy gained is of this order, the speckle cross section decreases rapidly, and the heating is cut off. Expressed in terms of intensity for $\lambda_0 = 1$ μm, the energy gained is $E \approx 1.44(I/10^{18}\ \mathrm{W\,cm^{-2}})^{1/2}$ MeV, which is close to the well-known relativistic scaling [35] $E \approx 1.5(I/10^{18}\ \mathrm{W\,cm^{-2}})^{1/2}$ MeV observed in a variety of simulations and experiments [13–17]. The stochastic nature of the acceleration is expected to give rise to quasithermal electron spectra, and in Fig. 5 we show our analytic scaling alongside the simulation results, with good agreement in the relativistic regime. Electron-speckle scattering therefore offers an alternative explanation for the hot electon temperatures observed at high intensity.

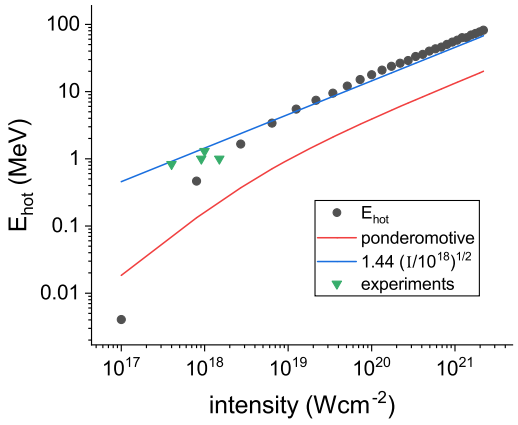

FIG. 5. Hot electron energy scaling with intensity from simulations with 300 fs pulses (black dots). The ponderomotive scaling is shown in red, alongside our analytic expression $E \approx 1.44(I/10^{18}\ \mathrm{W\,cm^{-2}})^{1/2}$ MeV in blue and recent experiments (green).

In summary, we have shown that the ponderomotive force generated by laser speckles can scatter electrons in much the same way as electron-ion Coulomb scattering. The scattering rate $\nu \propto I^2/R$ can exceed the Coulomb scattering rate in some important laser-plasma interaction applications, and this will lead to significant corrections to plasma transport properties. At intensities approaching relativistic, $I \gtrsim 10^{17}(\lambda_0/1\ \mu\mathrm{m})^2\ \mathrm{W\,cm^{-2}}$, electron scattering in speckles results in large energy gains with characteristic hot electron temperature scaling as $E \approx 1.44(I/10^{18}\ \mathrm{W\,cm^{-2}})^{1/2}$ MeV.

We gratefully acknowledge useful discussions with W. Rozmus, M. Belyaev, J. Ludwig, L. Divol, E. Kur, T. Chapman, M. Tabak, M. Rosen, D. Strozzi, A. Kemp, S. C. Wilks, and W. Kruer. This work was performed under the auspices of the U.S. Department of Energy by the Lawrence Livermore National Laboratory under Contract No. DE-AC52-07NA27344. This document was prepared as an account of work sponsored by an agency of the United States government. Neither the United States government nor Lawrence Livermore National Security, LLC, nor any of their employees makes any warranty, expressed or implied, or assumes any legal liability or responsibility for the accuracy, completeness, or usefulness of any information, apparatus, product, or process disclosed, or represents that its use would not infringe upon privately owned rights. References herein to any specific

commercial product, process, or service by trade name, trademark, manufacturer, or otherwise does not necessarily constitute or imply its endorsement, recommendation, or favoring by the United States government or Lawrence Livermore National Security, LLC. The views and opinions of the authors expressed herein do not necessarily state or reflect those of the United States government or Lawrence Livermore National Security, LLC, and shall not be used for advertising or product endorsement purposes. IM release LLNL-JRNL-832284.

Appendix A: The average over the speckle intensity distribution.—The analysis in the main text considers electrons interacting with speckles of fixed intensity, but in reality a beam contains a statistical distribution of intensities, which can be described by a probability (P) density function $dP/du = p(u)$, where $u = I/I_0$ is the speckle intensity normalized to the beam average I_0. We use a slightly modified form of Garnier's expression [36] for the probability density: $p(u) = Ae^{u_c-u}(20u^2 - 36u + 3)/2u^{1/2}$ with $\int_{u_c}^{\infty} p(u)du = 1$ and $A = [3(7\sqrt{66} + 57)]^{-1/2}$. The modification simply excludes negative values of the probability, which only occur at low intensities $u < u_c = (9 + \sqrt{66})/10 \approx 1.7$. This introduces negligible error in our calculations because the higher intensity speckles, in the range $2 \lesssim u \lesssim 7$, dominate the scattering. When the number density of speckles is expressed as a probability, the rates are given by integrals over u in the form $\upsilon(v) = \int G(v,u)p(u)du$ because the number density of speckles within du of u is $dn_A = A_{\rm sp}^{-1}p(u)du$, with $A_{\rm sp} = \pi R^2$ the speckle cross sectional area. To carry out this integral, the approximate rates $\tilde{\nu}_i$ are first expressed in terms of u and w by using $v_{\rm osc} = u^{1/2}v_0$ and $w = \bar{v}/u^{1/2}$, where v_0 is the value of $v_{\rm osc}$ when $u = 1$ (i.e., v_0 is the oscillatory velocity when $I = I_0$) and $\bar{v} = v/v_0$. The intensity-weighted momentum-loss collision rate is given by $\tilde{\nu}_{p,c}(\bar{v}) = \int[\tilde{\nu}_{p,c}(\bar{v},u)/n_A]dn_A = \int_{u_c}^{\infty}\tilde{\nu}_{p,c}(\bar{v},u)p(u)du$, where the function in the integrand $f(\bar{v},u) = \tilde{\nu}_{p,c}(\bar{v},u)p(u)$ is

$$f(\bar{v},u) = \frac{2Ae^{u_c-u}u^{3/2}(20u^2 - 36u + 3)\bar{v}v_0A_{\rm sp}^{-1}R}{3(20\bar{v}^4 + u^2)}. \quad \text{(A1)}$$

This function can be approximated in the low velocity "L" ($\bar{v} \ll 1$) and high velocity "H" ($\bar{v} \gg 1$) limits by replacing the denominator term with $20\bar{v}^4 + u^2 \approx u^2$ and $20\bar{v}^4 + u^2 \approx 20\bar{v}^4$, respectively, giving functions in both limits: $f_L = 2Ae^{u_c-u}(20u^2 - 36u + 3)\bar{v}v_0A_{\rm sp}^{-1}R/3u^{1/2}$ and $f_H = Ae^{u_c-u}u^{3/2}(20u^2 - 36u + 3)\bar{v}^{-3}v_0A_{\rm sp}^{-1}R/30$. Carrying out the integrals of these approximate functions gives the total collision rate in the low ("L") and high ("H") velocity limits: $\tilde{\nu}_{p,c}(\bar{v})_L = (4/3)\bar{v}v_0$ and $\tilde{\nu}_{p,c}(\bar{v})_H = (B_c/1500)\bar{v}^{-3}v_0^4$ where $B_c = 308\sqrt{66} - 793 + 220e^{u_c}\sqrt{5(57-7\sqrt{66})\pi}\,\mathrm{Erfc}(u_c)$ and $\mathrm{Erfc}(x)$ is the complementary error function. Since the approximations $\tilde{\nu}_{p,c}(\bar{v})_L$ and $\tilde{\nu}_{p,c}(\bar{v})_H$ have the same functional form with respect to $\bar{v}$ as does $\tilde{\nu}_{p,c}(w)$ with respect to w, we can use the same technique as shown in the main text to combine both limits in a single approximate function again of the form $g(\bar{v})$. This yields

$$\tilde{\nu}_{p,c}(v) = \frac{4}{3\pi R}\frac{v}{1 + a_c(v/v_0)^4} \quad \text{(A2)}$$

where $a_c = 2000/[308\sqrt{66} - 793 + 220e^{u_c}\sqrt{5(57-7\sqrt{66})\pi}\,\mathrm{Erfc}(u_c) - 793] \approx 1.1$. We have numerically verified good accuracy of Eq. (A2) in the $v \ll 1$ and $v \gg 1$ limits.

A guide to the parameters used in the main text to calculate the scattering angle is shown in Fig. 6.

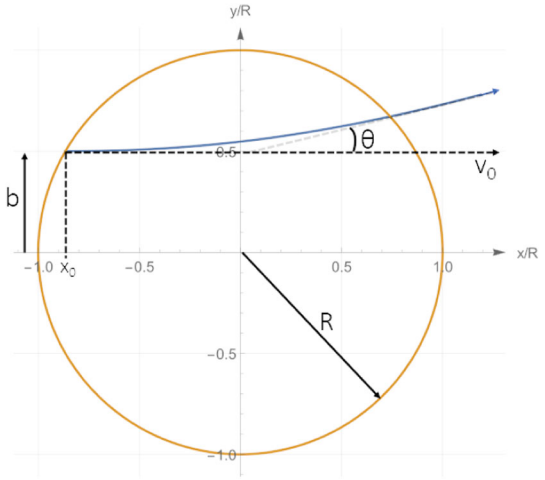

FIG. 6. Schematic diagram showing the key parameters in the analytic treatment of an electron interacting with a speckle of radius R.

Appendix B: The average over a Maxwellian.—The expression in Eq. (1) can be averaged over a Maxwellian velocity distribution $4\pi(2\pi v_t^2)^{-3/2}\exp(-v^2/2v_t^2)$, where $v_t = \sqrt{T_e/m_e}$ to obtain the thermal collision rate $\nu_{p,c,M} = \sqrt{2}H_K v_0^4/(3\pi^{3/2}a_c R v_t^3)$, where $H_K = [\pi - 2\mathrm{Si}(K)]\sin(K) - 2\mathrm{Ci}(K)\cos(K)$, $K = v_0^2/(2\sqrt{a_c}v_t^2)$, the sine integral is $\mathrm{Si}(x) = \int_0^x t^{-1}\sin(t)dt$, and the cosine integral is $\mathrm{Ci}(x) = \int_0^x t^{-1}\cos(t)dt$. In most experimental regimes of interest, $K \ll 1$ so this can be simplified to $\nu_{p,c,M} \approx 2\sqrt{2}\ln(K^{-1})v_0^4/(3\pi^{3/2}a_c R v_t^3)$. Note that this is a similar form to the Coulomb scattering rate, but with the replacement $Z^2 n_i \ln\Lambda \to I^2 R^{-1}\ln K^{-1}$.

Appendix C: Relativistic theory.—In the ultrarelativistic limit (Lorentz factor $\gamma \gg 1$), the ponderomotive force is $\boldsymbol{F}_p = -(c/\sqrt{2})\nabla p_{\rm osc}$, where $p_{\rm osc} = eE_0(\mathbf{r})/\omega_0$ is the oscillatory momentum [37]. This allows us to write the ultrarelativistic ponderomotive potential as $\varphi_p = p_{\rm osc}c/\sqrt{2}$. The equation of motion of an electron interacting with this potential is therefore $d\mathbf{p}/dt = -\nabla\varphi_p$, with $\mathbf{p} = \gamma m d\mathbf{r}/dt$. We make the simplifying assumption, common in relativistic mechanics, that the Lorentz factor is approximately constant during the interaction $\gamma \approx \gamma_0$, so that $d^2\mathbf{r}/dt^2 = -(c/\sqrt{2}m\gamma_0)\nabla p_{\rm osc}$. We again assume a parabolic potential profile, and if we define a new velocity variable $u_{\rm osc} = (4p_{{\rm osc},0}c/\sqrt{2}m\gamma_0)^{1/2}$, the equation of motion becomes identical to the nonrelativistic case with the replacement $v_{\rm osc} \to u_{\rm osc}$. The solutions are then $x(t) = -\frac{1}{2}(e^{\omega t} + e^{-\omega t})x_0 + \frac{1}{2}(e^{\omega t} - e^{-\omega t})(p_{x0}R\omega/p_{{\rm osc},0}c)$ and $y(t) = \frac{1}{2}b(e^{\omega t} + e^{-\omega t})$, where $\omega = (2^{1/4}/R)\sqrt{(p_{{\rm osc},0}c/\gamma_0 m)}$. We have verified that the assumption $\gamma \approx \gamma_0$ is good by comparing this analytic solution for the trajectory to fully relativistic numerical calculations. Following along the nonrelativistic derivation, but with these new variables, we find $\tilde{\nu}_{p,s} \simeq \pi R^2 n u_{\rm osc}\bar{v}/(1 + 12\bar{v}^4)$, where $\bar{v} = {\rm v}/u_{\rm osc}$, which characterizes the electron momentum relative to the oscillatory momentum, since $\bar{v}^2 = ({\rm v}/u_{\rm osc})^2 = (\sqrt{2}/4)({\rm v}/c)(p_{x0}/p_{{\rm osc},0}) \approx p_{x0}/p_{{\rm osc},0}$. The integral over the intensity distribution is similar to the nonrelativistic case except that we take into account the fact that the scaling with u is now $u_{\rm osc} = u^{1/4}u_0$ and $w = \bar{v}/u^{1/4}$. These changes lead to the relativistic collision rate

$$\tilde{\nu}_{p,s,{\rm rel}}(v) = \frac{3}{4R}\frac{v}{1 + a_s(v/u_0)^4} \tag{C1}$$

with $a_s \approx 3.0$.

The solutions to the equations of motion of an electron in a plane electromagnetic wave have been obtained by many authors in terms of the proper time (e.g., Refs. [38,39]). To obtain useable expressions for the electron momentum $\boldsymbol{u}$, valid for times short compared to the oscillation period, we Taylor expand Yang's [39] expressions in time to first order, which results in

$$u_x \simeq u_{x0} - a_0\Delta c \tag{C2}$$

$$u_z \simeq \frac{1 + u_{x0}^2 - 2a_0u_{x0}\Delta c}{2\alpha_0} - \frac{\alpha_0}{2} \tag{C3}$$

where u_x is the momentum in the direction of laser polarization in units of mc (initially $= u_{x0}$), u_z is the momentum in the direction of laser propagation in units of mc (initially $= u_{z0}$), $\alpha_0 = \gamma_0 - u_{z0}$, $\gamma_0 = \sqrt{1 + u_x^2 + u_z^2}$, $\Delta c = t(\omega_0 - kv_{z0})\sin(kv_{z0})$, $v_{z0} = u_{z0}/\gamma_0$, $a_0 = eE_0/mc\omega_0$ is the normalized wave amplitude, and k is the wave number. Note that here the symbol u refers to the *normalized* momentum. The square change in momentum $\boldsymbol{\Delta}(u^2) = (u_x - u_{x0})^2 + (u_z - u_{z0})^2$ after time t is

$$\boldsymbol{\Delta}(u^2) = a_0^2t^2(\omega_0 - kv_{z0})^2\sin^2(kv_{z0}) + \left\{\frac{1 + u_{x0}^2 - 2u_{x0}a_0t(\omega_0 - kv_{z0})\sin(kv_{z0})}{2\alpha_0} - \frac{\alpha_0}{2} - u_{z0}\right\}^2. \tag{C4}$$

Assuming the electron momentum distribution function is initially isotropic in the $x - z$ plane, we adopt a polar coordinate system $u_0 = \sqrt{u_{x0}^2 + u_{z0}^2}$, $u_{x0} = u_0\sin\theta$, $u_{z0} = u_0\cos\theta$ and average $\boldsymbol{\Delta}(u^2)$ over all angles θ to obtain

$$\boldsymbol{\Delta}(u^2) = \frac{a_0^2t^2(1 + 2u_0^2)^2\sin^2(\varphi_{z0})}{1 + u_0^2} \tag{C5}$$

where $\varphi_0 = -kv_{z0}$ is the initial phase. We carry out the trivial average over all initial phases φ_0, assuming electrons are initially evenly distributed along the wave axis. Further assuming an initially thermal distribution characterized by a thermal momentum u_t, of the form $f(u_0) = \sqrt{(2/\pi)}u_t^{-3}\exp(-u_0^2/2u_t^2)$ we can calculate the average $\langle\boldsymbol{\Delta}(u^2)\rangle = \int_0^\infty \boldsymbol{\Delta}(u^2)f(u_0)u_0^2du_0$:

$$\langle\boldsymbol{\Delta}(u^2)\rangle = \frac{a_0^2t^2}{4u_t^3}\left\{\sqrt{2\pi}{\rm Erfc}\left(\frac{1}{\sqrt{2}u_t}\right) + 4u_t^3 - 2u_t\right\}. \tag{C6}$$

If the electrons are initially cold, $u_t \ll 1$, then we obtain the scaling $\sqrt{\langle\boldsymbol{\Delta}(u^2)\rangle} \simeq a_0t/2$, which agrees well with numerical simulations for short times. Note that a similar scaling can be found for exponential energy distributions. This scaling is used to estimate the energy gain of a cold isotropic distribution of electrons in a wave.

[1] S. I. Braginskii, Rev. Plasma Phys. **1**, 205 (1965).

[2] Y. Kato, K. Mima, N. Miyanaga, S. Arinaga, Y. Kitagawa, M. Nakatsuka, and C. Yamanaka, Phys. Rev. Lett. **53**, 1057 (1984).

[3] S. Skupsky, R. W. Short, T. Kessler, R. S. Craxton, S. Letzring, and J. M. Soures, J. Appl. Phys. **66**, 3456 (1989).

[4] P. Michel, L. Divol, E. A. Williams, S. Weber, C. A. Thomas, D. A. Callahan, S. W. Haan, J. D. Salmonson, S. Dixit, D. E. Hinkel, M. J. Edwards, B. J. MacGowan, J. D. Lindl, S. H. Glenzer, and L. J. Suter, Phys. Rev. Lett. **102**, 025004 (2009).
[5] S. H. Glenzer *et al.*, Science **327**, 1228 (2010).
[6] W. L. Kruer, S. C. Wilks, B. B Afeyan, and R. K. Kirkwood, Phys. Plasmas **3**, 382 (1996).
[7] E. A. Williams, Phys. Plasmas **13**, 056310 (2006).
[8] D. H. Froula, L. Divol, N. B. Meezan, S. Dixit, J. D. Moody, P. Neumayer, B. B. Pollock, J. S. Ross, and S. H. Glenzer, Phys. Rev. Lett. **98**, 085001 (2007).
[9] G. J. Pert, J. Phys. A A **5**, 506 (1972).
[10] O. S. Jones, L. J. Suter, H. A. Scott, M. A. Barrios, W. A. Farmer, S. B. Hansen, D. A. Liedahl, C. W. Mauche, A. S. Moore, M. D. Rosen, J. D. Salmonson, D. J. Strozzi, C. A. Thomas, and D. P. Turnbull, Phys. Plasmas **24**, 056312 (2017).
[11] J. P. Brodrick, R. J. Kingham, M. M. Marinak, M. V. Patel, A. V. Chankin, J. T. Omotani, M. V. Umansky, D. Del Sorbo, B. Dudson, J. T. Parker, G. D. Kerbel, M. Sherlock, and C. P. Ridgers, Phys. Plasmas **24**, 092309 (2017).
[12] P. M. Woodward and J. D. Lawson, J. Inst. Electr. Eng. **95**, 363 (1948).
[13] H. Chen, S. C. Wilks, J. D. Bonlie, E. P. Liang, J. Myatt, D. F. Price, D. D. Meyerhofer, and P. Beiersdorfer, Phys. Rev. Lett. **102**, 105001 (2009).
[14] H. Chen, A. Link, Y. Sentoku, P. Audebert, F. Fiuza, A. Hazi, R. F. Heeter, M. Hill, L. Hobbs, A. J. Kemp, G. E. Kemp, S. Kerr, D. D. Meyerhofer, J. Myatt, S. R. Nagel, J. Park, R. Tommasini, and G. J. Williams, Phys. Plasmas **22**, 056705 (2015).
[15] H. Chen, F. Fiuza, A. Link, A. Hazi, M. Hill, D. Hoarty, S. James, S. Kerr, D. D. Meyerhofer, J. Myatt, J. Park, Y. Sentoku, and G. J. Williams, Phys. Rev. Lett. **114**, 215001 (2015); G. J. Williams *et al.*, Phys. Rev. E **101**, 031201(R) (2020).
[16] D. Mariscal *et al.*, Phys. Plasmas **26**, 043110 (2019).
[17] D. R. Rusby *et al.*, Phys. Rev. E **103**, 053207 (2021).
[18] L. Spitzer, *Physics of Fully Ionized Gases*, 2nd Revised ed. (Dover Publications Inc., Mineola, New York, 1990).
[19] See Supplemental Material at http://link.aps.org/supplemental/10.1103/PhysRevLett.129.215001 for a derivation of the scattering rate for spherical speckles, which closely follows the cylindrical case and results in the same functional form but with modified constants; a description of time-dependent kinetic simulations that include the effects of SSD, inverse bremsstrahlung absorption and nonlocal heat flow; and the average over a Maxwellian velocity distribution for spherical speckles, which has the same functional dependence on variables as the cylindrical case and a comparable magnitude, which includes Refs. [20–25].
[20] J.-L. Feugeas, Ph. Nicolai, X. Ribeyre, G. Schurtz, V. Tikhoncuk, and M. Grech, Phys. Plasmas **15**, 062701 (2008).
[21] A. R. Bell, A. P. L. Robinson, M. Sherlock, R. J. Kingham, and W. Rozmus, Plasma Phys. Controlled Fusion **48**, R37 (2006).
[22] M. Sherlock, J. P. Brodrick, and C. P. Ridgers, Phys. Plasmas **24**, 082706 (2017).
[23] T. D. Arber and R. G. L. Vann, J. Comput. Phys. **180**, 339 (2002).
[24] A. B. Langdon, Phys. Rev. Lett. **44**, 575 (1980).
[25] V. Yu. Bychenkov, J. Myatt, W. Rozmus, and V. T. Tikhonchuk, Phys. Plasmas **1**, 2419 (1994).
[26] P. Michel, W. Rozmus, E. A. Williams, L. Divol, R. L. Berger, S. H. Glenzer, and D. A. Callahan, Phys. Plasmas **20**, 056308 (2013).
[27] R. Sentis, S. Desroziers, and F. Nataf, Simulation of laser propagation in a plasma with a frequency wave equation, in *Proceedings of VECPAR'06*, edited by M. Dayde *et al.* (Springer, Berlin, 2007), pp. 518–529.
[28] E. M. Epperlein, Phys. Rev. Lett. **65**, 2145 (1990).
[29] S. C. Wilks, W. L. Kruer, M. Tabak, and A. B. Langdon, Phys. Rev. Lett. **69**, 1383 (1992).
[30] C. S. Brady, A. Lawrence-Douglas, and T. D. Arber, Phys. Plasmas **19**, 063112 (2012).
[31] M. Tabak, J. Hammer, M. E. Glinksy, W. L. Kruer, S. C. Wilks, J. Woodworth, E. M. Campbell, M. D. Perry, and R. J. Mason, Phys. Plasmas **1**, 1626 (1994).
[32] J. S. Green *et al.*, Phys. Rev. Lett. **100**, 015003 (2008).
[33] J. Meyer-ter-Vehn and Z.-M. Sheng, Phys. Plasmas **6**, 641 (1999).
[34] Z.-M. Sheng, K. Mima, Y. Sentoku, M. S. Jovanovic, T. Taguchi, J. Zhang, and J. Meyer-ter-Vehn, Phys. Rev. Lett. **88**, 055004 (2002).
[35] A. Pukhov, Z.-M. Sheng, and J. Meyer-ter-Vehn, Phys. Plasmas **6**, 2847 (1999).
[36] J. Garnier and L. Videau, Phys. Plasmas **8**, 4914 (2001).
[37] E. Esarey, P. Sprangle, J. Krall, and A. Ting, IEEE Trans. Plasma Sci. **24**, 252 (1996).
[38] M. G. Haines, M. S. Wei, F. N. Beg, and R. B. Stephens, Phys. Rev. Lett. **102**, 045008 (2009).
[39] J.-H. Yang, R. Craxton, and M. G. Haines, Plasma Phys. Controlled Fusion **53**, 125006 (2011).